Fast prediction of antibiotic permeability through membrane channels using Brownian dynamics

Acharya, Abhishek; Jana, Kalyanashis; Gurvic, Dominik; Zachariae, Ulrich; Kleinekathöfer, Ulrich

Published in:
Biophysical Journal

DOI:
10.1016/j.bpj.2023.03.035

Publication date:
2023

Manuscript submitted to **Biophysical***Journal*
Article

Fast Prediction of Antibiotic Permeability through Membrane Channels using Brownian Dynamics

Abhishek Acharya[1], Kalyanashish Jana[1], Dominik Gurvic[2], Ulrich Zachariae[2], and Ulrich Kleinekathöfer[1,*]

[1]School of Science, Constructor University, Campus Ring 1, 28759 Bremen, Germany
[2]School of Life Sciences, University of Dundee, Dow Street, Dundee DD1 5EH, United Kingdom
[*]Correspondence: ukleinekathoefer@constructor.university

ABSTRACT The efficient permeation across the Gram-negative bacterial membrane is an important step in the overall process of antibacterial action of a molecule and the one that has posed a significant hurdle on the way towards approved antibiotics. Predicting the permeability for a large library of molecules and assessing the effect of different molecular transformations on permeation rates of a given molecule is critical to the development of effective antibiotics. We present a computational approach for obtaining estimates of molecular permeability through a porin channel in a matter of hours using a Brownian dynamics approach. The fast sampling using a temperature acceleration scheme enables the approximate estimation of permeability using the inhomogeneous solubility diffusion model. Though the method is a significant approximation to similar all-atom approaches tested previously, we show that the present approach predicts permeabilities that correlate fairly well with the respective experimental permeation rates from liposome swelling experiments and accumulation rates from antibiotic accumulation assays, and is significantly, i.e., about 14 times, faster compared to a previously reported approach. The possible applications of the scheme in high-throughput screening for fast permeators are discussed.

SIGNIFICANCE Fast prediction of solute permeability through channels such as bacterial porins is useful in the design and screening of new antibiotics with improved influx into Gram-negative bacterial cell. We employ a fast Brownian dynamics-based approach to obtain estimates of single channel permeability for molecules at a significantly lower computational cost.

INTRODUCTION

Investigations of the process of drug uptake and accumulation within Gram-negative bacterial cells through outer membrane pores holds the promise of enabling the development of more effective antibacterial molecules. Over the past couple of decades, experimental and computational approaches have provided a deeper understanding of the antibiotic permeation process through porin channels that act as major translocation route across the bacterial outer membrane for several antibiotics (1–8). These studies have enabled the derivation of a variety of permeation rules that can guide the design of antibiotic molecules with improved permeation rates (9–11). The generation of more effective antibiotic candidates has become possible through the application of such rational rules, as has been demonstrated in recent studies (12–14). For example, a FabI inhibitor was recently carefully redesigned to generate variants containing a primary amino group and subsequently screened to identify the ones with strong affinity to the intracellular target (15). Notably, the data on accumulation and MIC of the designed variants suggests that introducing a primary amine to improve antibiotic permeation rates may be necessary but not sufficient to ensure good antimicrobial activity, and any redesign strategy must also carefully optimize the binding affinity to the intracellular target protein. Nonetheless, a useful strategy that has emerged from these works involves careful redesigning that introduces a primary amine moiety to existing antibiotic scaffolds to generate variants that are subsequently screened for improved antibacterial activity. Moreover, a recent study used a deep neural network model (16, 17) and matched molecular pair analysis (18) on a database of molecules active against Gram-positive and Gram-negative bacteria to uncover pairs of chemical transformations that are linked to improved efficacy against Gram-negative bacterial pathogens (19). While it is still not clear whether the suggested transformations are connected to improved influx rates or the binding affinity to the target, a plausible redesign strategy could introduce some validated transformations to generate a large set of candidate molecules. Subsequently, such

candidate libraries need to be screened for improved permeability and antimicrobial activity. High-throughput screening of a large library of compounds for efficient permeators is thus expected to become a useful strategy for supporting the initial screening step as well as subsequent optimization steps. A number of efforts has already sought to develop strategies for the experimental determination of molecular permeability through porins (8). However, each of these strategies has been faced with different challenges and sources of error in accurately quantifying channel mediated transport. Moreover, the experimental estimation of drug permeability remains a resource-intensive approach that precludes high-throughput screening of a drug library.

Computational approaches have also been developed for the prediction of free energy surfaces and estimation of antibiotic permeabilities (8, 20). For estimating permeability coefficients for antibiotics through a channel, these methods make use of the inhomogeneous solubility diffusion (ISD) model (21) that estimates the permeability coefficient from the calculated one-dimensional free energy estimates $F(z)$ along the channel axis z and the position dependent diffusivity $D(z)$ of the solute (see equation 6 in the Methods section). However, in practice the calculation of the two quantities from simulations is challenging, especially in simulations of large antibiotic molecules within porin channels (10). While a number of approaches employ enhanced sampling schemes to estimate $F(z)$ and $D(z)$, fast estimation of permeability coefficients for a library of molecules still remains beyond reach. For instance, a recent work used the umbrella sampling method for estimating permeabilities of 14 antibiotics that correlated with the experimental values obtained from outer membrane vesicle (OMV) swelling assays (22). It was reported, however, that the calculations required 1.1 μs simulations per molecule and needed about a week to finish. A more approximate approach has considered an expression for the permeability coefficient that included only terms relevant to the constriction region of the channel, based on the assumption that the permeation rate is dominated by the energetic barrier and the effective diffusion rate at the constriction region (10). There is a need for methods that can provide initial predictions of antibiotic permeability through porins, much like ligand-docking approaches in the prediction of strong binders taking.

Simulations employing an implicit, continuum or a coarse-grained treatment of the system or components thereof provide a computationally feasible alternative to full atomistic approaches (23–30). In particular, Brownian dynamics simulations are suitable for the study of solute transport processes through membrane pores over longer time scales (23–26, 31, 32). In previous studies, we have used a Brownian dynamics approach for the study of antibiotic permeation though porins. Specifically, the Brownian dynamics with explicit atoms (BRODEA) approach was employed to obtain the energetics of the antibiotic permeation process, and recover permeation behavior in agreement with atomistic molecular dynamics and reported experimental data (33, 34). It was demonstrated also that a combination of the BRODEA scheme with temperature accelerated molecular dynamics (TAMD) approach - the so-called temperature accelerated Brownian dynamics (TABD) method - enables a qualitative description of antibiotic translocation and the determination of an approximate free energy surface for the permeation process (33). More recently, the TABD scheme has been used in combination with electrophysiological experiments to obtain insights into the plausible permeation pathways for norfloxacin through four different porins and to examine the effect of divalent cations on the permeation behavior of these channels (35). Here we present a fast and straightforward approach for obtaining estimates for permeability of antibiotic molecules through a given channel using microsecond-long TABD simulations. The present approach introduces some additions to the original BRODEA setup by enabling the automated preparation of multiple initial input states with different pore and antibiotic configurations as opposed to the previous reports that used a single static pore configuration. We used TABD simulations to estimate the permeabilities for a set of molecules permeating through the OmpF channel and find that the approach is able to fairly well reproduce the trend in experimental permeability obtained from liposome-swelling assays. Furthermore, simulations on molecules with reported accumulation rates show that the estimated permeabilities for these molecules are generally correlated with the experimentally observed accumulation rates. Notably, our results indicate that the approach may be able to identify cases in which the experimental data may be unreliable owing to limitations of the assay design. Finally, we have examined the performance of the method in predicting the effect of chemical modifications on the permeability of the transformed molecule - one of the potential practical use cases of such a method. Taking examples of transformation pairs that involve the introduction of a primary amine, we show that the method is able to predict for most cases a relative increase in permeation rate on the introduction of a primary amine.

METHODS

Temperature Accelerated Brownian Dynamics Method

BRODEA simulations have been performed wherein the whole system is decomposed into an implicit component and an explicit set of particles. The implicit region typically includes the protein and the membrane that are kept at fixed positions, that is, not propagated in time. The explicit atoms are essentially treated as Brownian particles that are evolved using the overdamped Langevin equation of motion (24, 26). Moreover, the solvent is treated as continuum dielectric. For the N Brownian particles the forces are obtained from the negative gradient of a many-body potential energy function, given by (1), that includes the

appropriate terms for modeling the bonded and non-bonded interactions of the explicit region, as well as the non-bonded electrostatic and reaction-field terms plus steric repulsive potential terms from the implicit components (33).

$$
\begin{aligned}
U(\boldsymbol{x}^N) = \Bigg\{ & \sum_{\text{bonds}} \kappa_b (b - b_0)^2 + \sum_{\text{angles}} \kappa_\theta (\theta - \theta_0)^2 + \sum_{\text{Urey-Bradley}} \kappa_s (s - s_0)^2 \\
& + \sum_{\text{dihedrals}} \kappa_\varphi (1 - \cos(n\varphi - \delta)) + \sum_{\text{impropers}} \kappa_\omega (\omega - \omega_0)^2 \\
& + \sum_{\text{residues}} U_{\text{CMAP}} \Bigg\}_{\text{bonded}} \\
& + \Bigg\{ \sum_{i}^{N} \left[q_i \left[\phi_{sf}(\boldsymbol{x}_i) + \frac{\phi_{rf}(\boldsymbol{x}_i)}{2} \right] + U_{\text{core}}(\boldsymbol{x}_i) \right] \\
& + \sum_{j>i}^{N} \left[4\epsilon_{ij} \left[\left(\frac{\sigma_{ij}}{r_{ij}} \right)^{12} - \left(\frac{\sigma_{ij}}{r_{ij}} \right)^{6} \right] + w_{\text{sr}}(r_{ij}) + \frac{q_i q_j}{4\pi\epsilon_0 \epsilon_{bulk} r_{ij}} \right] \Bigg\}_{\text{non-bonded}} .
\end{aligned}
\tag{1}
$$

Here, the bonded terms include the potential energy contributions from bonds, angles, dihedrals and improper dihedral angles as defined in the CHARMM force field (36). Additionally, Urey-Bradley terms for the bond-angle vibration between atom triplets are also included as are the CMAP corrections U_{CMAP} to torsional energies. The non-bonded energy terms are sums over the N Brownian particles and include the electrostatic contributions from the implicit protein charges and the transmembrane potential ϕ_{sf}, the reaction field contributions arising from the dielectric heterojunction between protein, membrane and solvent regions ϕ_{rf}, and the repulsive core steric potential from the protein and membrane parts. Also included are the pair-wise Lennard-Jones contributions, a water-mediated short-range term w_{sr} and Coulombic electrostatic terms. We have used the combination of BD with periodic boundary conditions (PBC) that is conceptually simpler and computationally less expensive than the grand canonical Monte Carlo-based BD (GCMC/BD) scheme (23). Details of the BRODEA method and its implementation are discussed elsewhere (32–34).

Sampling of solute configurations are often problematic due to free energy barriers larger than thermal energy leading to an extremely low probability of transitions between the important free energy basins along the reaction coordinate. Typically, for enhancing the sampling along the reaction coordinate, a low-dimensional coarse description of the reaction coordinate is employed. One or a set of collective variables (CVs) are chosen that are functions of the atomic Cartesian coordinates and suitable for describing the process under investigation. The complete sampling in this CV space is expected to adequately describe the process. Presently, we employ temperature acceleration to improve sampling of the solute configurations within the protein channel during the BRODEA simulations. This so-called temperature accelerated molecular dynamics (TAMD) scheme as introduced by Maragliano and Vanden-Eijnden attempts to improve sampling in the chosen CV space by using a higher than normal temperature (37). The method has been used previously in combination with other biasing schemes to improve the sampling efficiency in the study of a number of biologically important processes including antibiotic permeation through porins (38–41). Briefly, the TAMD scheme uses an extended Lagrangian framework and introduces additional dynamical variables s_i that are coupled tightly to the original (real) CVs $S_i(\boldsymbol{r}^N)$. The introduced fictitious variables are coupled to a separate temperature bath maintained at a higher temperature relative to the system temperature. Under the imposed conditions of adiabatic decoupling, the fictitious variables are evolved using a high temperature that in turn drive the coupled real CVs, enabling improved sampling in the relevant CV space. The many-body potential energy function is thus modified as follows

$$
U(\boldsymbol{x}^N, \boldsymbol{s}) = U(\boldsymbol{x}^N) + \frac{1}{2} \sum_{j=1}^{m} \kappa_j (s_j - S_j(\boldsymbol{r}^N))^2 .
\tag{2}
$$

Here, κ_j denotes the set of coupling parameters and the evolution of the additional variables s_j in time is described by an overdamped Langevin dynamics. For sufficiently strong coupling constants and slow diffusion of s_j compared to real space CVs S_j, it has been shown that dynamics of the s_j is consistent with the probability density function $e^{-\tilde{\beta}F(z)}$. The free energy at the physical temperature can be recovered by a straightforward reweighting step (7).

Diffusion Model

Diffusion constants are critical parameters that appear in the equation for the Brownian dynamics

$$
\frac{d\boldsymbol{x}_i}{dt} = -\frac{D_i(\boldsymbol{x}_i)}{k_B T} \nabla_i \, U(\boldsymbol{x}^N) + \nabla_i \, D_i(\boldsymbol{x}_i) + \xi_i(t) .
\tag{3}
$$

Here, D_i denotes the self-diffusion constant for the Brownian particle i, U the potential energy function defined in equation (1), and ξ a noise term modeling the collisions of solvent molecules with the Brownian particles. In general, the diffusion constant of a spherical particle in any medium of viscosity η is given by the Stokes-Einstein equation

$$D = \frac{k_B T}{6\pi\eta R_a} \,. \tag{4}$$

Here, R_a denotes the radius of the spherical particle, k_B the Boltzmann constant and T the temperature. Note that while the expression is valid for a particle in bulk solvent regions, it does not capture the behavior of particles passing though a protein channel with nanoscale pore dimensions. As can be seen in Eq. (3), the choice of the diffusion constant affects the observed dynamics and thus the properties estimated from these Brownian dynamics simulations. Although the BRODEA code by default assumes the bulk diffusion rates, it is possible to scale down the bulk diffusion rates within the channel by supplying appropriate scaling factors that are calculated from the estimates of the position dependent diffusion constant for the given antibiotic inside the channel. The diffusion constants inside the channel can be estimated either from detailed MD simulations (42–44) or by using the hydrodynamic diffusion (HD) model (26, 33). In this work we employ the HD model because the MD approach is computationally infeasible for large sets of molecules, especially in case of bulky solutes such as antibiotics due to slow sampling.

For the HD model, the position-dependent diffusion constant along the z axis (aligned with the pore axis) is given by

$$D(z) = \frac{D_{bulk}}{A + B\exp(\rho(z)/C) + D\exp(\rho(z)/E)} \tag{5}$$

where $\rho(z) = R_h/R_{pore}(z)$ denotes the ratio of the hydrodynamic radius R_h and the z-dependent pore radius $R_{pore}(z)$, while A, B, C, D and E are a set of parameters (26). $R_{pore}(z)$ is estimated using the HOLE algorithm (45) while R_h is a constant for a given antibiotic that can be estimated, for instance, using HYDROPRO (46). The scaling factors calculated in this way are used to modify the solute diffusion constant inside the pore during BRODEA runs. However, in the simulations of large, multiatomic solutes, the application of the calculated scaling factors to each atom comprising the solute is not straightforward. Previously, we tested the single-atom scaling approach wherein the scaling factor is applied to a single atom nearest to the center of mass of the molecule (34). Another approach tested was mass-weighted multiatom scaling wherein the scaling factor is distributed to all solute atoms using their masses as a weighting factor. The results suggested that both the methods perform similarly based on the comparison of free energy estimates obtained in BRODEA runs. In this study, we employ the single atom scaling approach due to its straightforward implementation within the BRODEA framework.

Simulation Setup

The system setup for TABD simulations is the same as elaborated in previous studies using the BRODEA scheme (32–34) and is described below. For the present work we have refactored and largely automated the setup procedure as described previously to enable TABD simulations on a large set of antibiotics.

Inputs

The TABD sampling data can be accrued from independent simulations that are run in parallel to expedite data collection. A simple setup script is used to prepare a user-specified number of independent runs. The script can accept a single input coordinate file with the channel and an antibiotic in an arbitrary position within the channel, and generates the required BRODEA input files for the independent simulations. This is referred to as the single configuration rigid implicit (SCRI) mode. Alternatively, the script can also accept a set of input coordinate files for the independent TABD runs, each with a potentially different input channel-antibiotic configuration. This is referred to as the multiple configuration rigid implicit (MCRI) mode that helps in partly compensating for the neglect of conformational flexibility of the channel. Here, “rigid implicit” specifies the implicit treatment of the protein channel. The input configurations for the channel can be chosen from an all-atom unbiased or biased MD simulations in combination with an appropriate clustering scheme. An antibiotic molecule can be inserted within the channel using the insert-molecules tool from the GROMACS package (47). The setup also requires as input the files specifying the CGENFF parameters for the antibiotic (prm and psf files). Finally, a setup parameter file specifying a number of directives for appropriate selection of the implicit and explicit parts as well as additional BRODEA and TABD run parameters need to be supplied.

Setup procedure

The first step involves the selection of the user specified channel residues and the antibiotic molecule out of the full all-atom coordinate files provided as input, followed by the reorientation of the selected coordinates to align the pore-axis to the z-axis,

and centering the channel COM at $z = 0$ Å. For the present runs, we select one full monomeric chain of OmpF and additional residues from the two other monomers (the loops L2 and L4, and turn T1) that also form a part of the selected channel. In the next step, the simulation box is constructed with a 40 Å wide implicit membrane around the monomer and a 20 Å thick slab of implicit water on both sides of the channel. The protein and the membrane parts are modeled as low dielectric regions with a dielectric constant of 2, and the implicit water with a dielectric constant of 80 (24, 31, 34). Subsequently, the reaction field and electrostatic potential maps are calculated for the implicit protein component. The HD diffusion model was used for which additional calculations need to be performed using the HOLE algorithm (45) to obtain the position dependent radius of the channel. The hydrodynamic radius for the solute is calculated using HYDROPRO (46). For each antibiotic, we took advantage of a compute node enabling 192 parallel BRODEA simulations to obtain a total sampling equivalent to about 75 μs-long runs per antibiotic. 96 different pore conformations were used, and the simulations were started at the two different ends of the pore leading to 192 unlike starting configurations. Note that in many cases shorter TABD runs would also suffice, but for automation purposes we performed longer runs that ensure adequate sampling for all cases.

The antibiotic molecules were optimized using the M06/6-311+G(d,p) level of theory in aqueous phase using the SMD solvation model with the self-consistent reaction field method (48–51). Further, harmonic frequency calculations were also carried out to examine the minima of the optimized geometries with no imaginary frequencies. The geometry optimizations and frequency calculations were performed using the Gaussian16 package (52). Subsequently, the optimized structures were used to produce CGenFF force field parameters using the ParamChem server (53, 54). The CHARMM stream files generated using ParamChem were further converted to a Gromacs-compatible topology file using a python script freely available on the web (55). In a next step, the optimized antibiotic structures were further employed in the MD setup. To this end, the antibiotic molecules were solvated using TIP3P water molecules, followed by an energy minimization using the steepest descent method. Then, short NVT and NPT equilibrium simulations were carried out and finally a 100 ns production run. The conformations obtained from these MD simulations have been structurally compared to the QM-optimized structures. This structural comparison and stability of the MD-generated conformations demonstrate the suitability of the newly determined force field parameters for the present application.

Torsional potential energy surface scanning

Furthermore, conformational analyses were carried out for the antibiotics cefamandole, cefsulodin, and piperacillin using the B3LYP/6-31+G(d,p) level of theory in the aqueous phase (56). The Gaussian16 package was used for the conformational study. The torsion angle α was allowed to change in 10° increments for the mentioned antibiotic molecules to explore the conformational flexibility on the potential energy surface along the selected torsions. The *ab initio* torsional angle distributions were further compared with the torsional distributions obtained from the BD simulation trajectories for these antibiotic molecules.

Estimation of Drug Permeability from BRODEA simulations

An estimate of the drug permeability through a single channel can be obtained using the inhomogeneous solubility diffusion (ISD) model (21). The approach attempts to model the solute permeation through a channel as a one-dimensional diffusion drift problem and has been employed in previous studies for estimating the permeability of solutes (10, 22). More precisely, the permeability coefficient for a drug through a channel can be estimated from the 1D free energy profile and the position-dependent diffusivity of the solute along the permeation coordinate z using the relation

$$\frac{1}{P_{\text{drug-channel}}} = \int \frac{e^{\,\beta F(z)}}{D(z)} dz \tag{6}$$

where $P_{\text{drug-channel}}$ is the permeability coefficient for a given drug and channel, β the inverse temperature, $F(z)$ the 1D free energy profile and $D(z)$ the position-dependent diffusion constant. As already mentioned, the estimation of $F(z)$ for an antibiotic permeation through a channel is particularly challenging and typically requires computationally intensive enhanced sampling schemes. Similarly, the estimation of $D(z)$ also requires an extensive sampling of the drug and channel configurations and thus previous approaches have sought to obtain both these quantities from a single set of biased simulations (57–60).

In the present approach, we estimate $F(z)$ from TABD simulations by a reweighting step

$$F(z) = -k_B \tilde{T}\ \ln(\tilde{P}(z)) \tag{7}$$

Here, $\tilde{T}$ is the artificial temperature used for accelerated sampling and $\tilde{P}(z)$ is the probability density function obtained from the TABD runs. Moreover, we employ an approximate estimate for $D(z)$ obtained using the equation for the hydrodynamic model provided in equation (5). The ratio $R_h/R_{pore}(z)$ is used to obtain an estimate for $D(z)$. For these simulations, the z region is

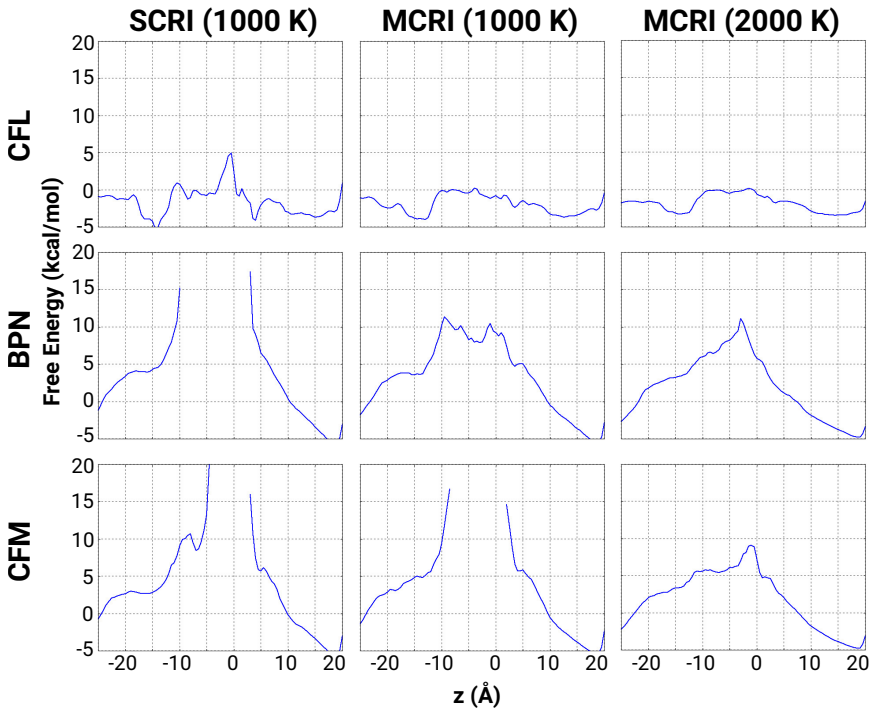

Figure 1: Free energy estimates obtained from temperature accelerated Brownian dynamics (TABD) simulations on three antibiotics cefaloridine (CFL), benzylpenicillin (BPN) and cefamandole (CFM). The left and the middle columns depict TABD simulations at 1000 K using the single-configuration rigid implicit (SCRI, left) scheme and the multi-configuration rigid implicit (MCRI, midlle) scheme . The MCRI simulations were also repeated at 2000 K (right column). In these plots, z denotes the center of mass distance between the antibiotic molecule and the channel. Gaps in the profiles indicate regions in which the free energy values were so high that a proper estimate was not possible.

chosen to be between the two channel ends, i.e., $z \in$ [-24Å , 20Å] assuming that the energetics and the diffusion behavior within the channel are the major contributing factors to the observed permeability.

The statistical error in the free energy estimates has been obtained using a bootstrapping approach where a fraction of the 192 walkers used for the BD simulations have been selected at random with replacement to create a bootstrap set. A total of 100 bootstrap free energy estimates have been obtained using this procedure and was used to obtain the standard deviations. Furthermore, for each free energy estimate obtained using this bootstrap scheme, a corresponding permeability rate has been calculated and used to obtain the average permeability rate and the associated standard deviation.

Selection of matched molecular pairs

To derive molecular pairs that increase in pMIC values through the gain of primary amine groups we analysed *E. coli* minimal inhibitory concentration (MIC) data from ChEMBL (61). Here, pMIC is defined as previously (19), i.e., pMIC= $-\log(\text{MIC}\ [\mu\ M]\ \text{x}\ 10^{-6})$. The data was curated to identical pMIC units; then mmpdb (62) was used to determine matched molecular pairs. Overall, we identified 895 molecular pairs (Fig. S1A) after filtering for molecular transformations that increase pMIC in a statistically significant way. Among these, 185 pairs exhibited a gain of a primary amine group after searching for substructural moieties using the approach from (19) (Fig. S1B). Ten examples were taken from that list to test the Brownian dynamics approach.

RESULTS AND DISCUSSION

Previously, multiple BRODEA simulations were run in parallel to obtain samples and each walker was initialized from the same initial configuration, that is, a single configuration scheme was used (33, 34). Here, in addition to the usual single configuration scheme (SCRI), we also tested a multiple configuration scheme (MCRI) wherein each simulation was started with a different protein conformation and antibiotic orientation. For initial validation, we worked with the permeability data on 12 antibiotics through the OmpF channel available from previous studies. Detailed information on the antibiotics are tabulated in Table 1.

Antibiotic	Charge	Mol. wt. (Da)	P_{exp} X 10^{-5}cm s^{-1}	P_{calc} X 10^{-5}cm s^{-1}	Relative error ($\Delta P_{calc}/P_{calc}$)
Cephaloridine	+ -	415	53.7 (63)	2.36 x 10^{-2}	0.27
Imipenem	+ -	299	17.5 (64)	4.58 x 10^{-3}	0.25
Cefazolin	-	453	15.8 (63, 65)	7.86 x 10^{-10}	0.82
Cephaloglycine	+ -	406	9.8 (63)	4.29 x 10^{-4}	0.65
Meropenem	+ -	383	3.0 (64)	1.65 x 10^{-3}	0.45
Cephalothin	-	395	2.9 (63)	9.40 x 10^{-8}	0.94
Piperacillin	-	516	2.7 (64)	1.44 x 10^{-7}	0.98
Cefsoludin	+ - -	531	1.8 (63)	N.A.	N.A.
Cefamandole	-	461	1.0 (63)	5.41 x 10^{-8}	0.77
Cephaloram	-	389	0.8 (63)	3.56 x 10^{-10}	0.80
Ampicillin	+ -	349	0.28 (66)	4.13 x 10^{-3}	0.36
Benzylpenicillin	-	333	0.07 (66)	3.47 x 10^{-9}	0.77

Table 1: Antibiotic permeabilities estimates from the TABD simulations together with their experimental counterparts (see the table for references) P_{exp} denotes the experimentally measured permeability rate and P_{calc} the permeability estimates determined from the TABD simulations. The charge column depicts the charged groups present in the antibiotic molecule.

The OmpF channel conformations used for the MCRI runs were obtained from a previous biased simulations of antibiotic permeation through OmpF (41). Specifically, we performed a K-means clustering using k=96 along a reduced two-dimensional PCA space. The PCA was performed on the pairwise distances between C-α of the L1 and the L3 loop that typically undergo the largest conformational fluctuations. The fluctuations in the rest of the channel were assumed to be largely captured in the clusters identified from the analysis; the overall objective was to sufficiently capture the possible protein conformations in the TABD simulations. Representative structures were extracted and used for preparation of the input antibiotic-OmpF coordinate files. Fig. 1 shows the free energies calculated for three representative molecules using TABD simulations at 1000 K. Comparing the results for the SCRI and MCRI schemes, we see that the choice of different initial configuration makes a noticeable difference to the sampling and consequently the final free-energy estimates obtained from TABD runs. Also note, in case of the cefamandole (CFM) antibiotic, we observed a lack of sampling in the central region of the channel at around $z = 0$, for both schemes. The central region is the constriction region (CR) of the channel that is characterized by a relatively narrow diameter and poses an entropic barrier to the passage of large antibiotics. Overall for the set of 12 antibiotics, 7 out of 12 antibiotics showed incomplete sampling in case of the SCRI scheme (Fig. S2). With the MCRI scheme, 3 antibiotics showed incomplete sampling along the channel translocation axis. It appears that the MCRI scheme offers a relatively better sampling of the CR compared to the SCRI scheme. Interestingly, for the antibiotics with incomplete sampling of the CR, we observed that the torsional space of the rotatable bonds of the antibiotic molecules are sampled adequately as evident from the torsional distributions observed in the BD simulations (Section S1 and Fig. S4-S6). The sampling issue appears to be largely due to the absence of protein dynamics in these simulations, that disallows antibiotic penetration into the CR. This is also apparent from the improvements observed for the MCRI scheme that considers an ensemble of protein structures. However, the lack for dynamical shift between antibiotic conformations and the associated transient protein backbone and side-chain conformations possibly precludes in these cases potential antibiotic-protein configurations important for the permeation process.

With the MCRI scheme, we observe incomplete sampling for the largest antibiotics in the set, namely cefamandole (CFM), cefsoludin (CFS) and piperacillin (PIP). Estimation of the full $F(z)$ energy profile is necessary for calculating the permeability coefficient using Eq. 6. We therefore performed TABD simulations at 2000 K with the expectation that a higher temperature, i.e., more energy in the system, could facilitate the penetration through the narrow CR. We find that increasing the temperature leads to an improved sampling along the translocation axis of the OmpF channel for all antibiotics except CFS (Fig. S2 and S3).

In a next step, we determined the permeability estimates according to Eq. 6 and the results are listed in Table 1 together the previously published experimental permeability data (22). It is important to point out that the experimental permeability coefficients in these studies are reported for a given antibiotic through a unit area of the respective bacterial membrane calculated using Fick's first law of diffusion, i.e., $J = -PA\Delta c$, where P denotes the permeability coefficient of the membrane, A the area of the membrane patch and Δc the difference in the solute concentrations of the two bulk reservoirs. The computational permeability estimates calculated using Eq. 6, however, denote the solute permeability through a single channel. Furthermore, the ISD approach used herein to obtain the theoretical estimates models the solute permeation behavior through the channel as a one dimensional diffusion drift problem and considers only the region that lies within the channel as the significant contributor to effective permeability to the solute. Thus, the permeability values obtained from theory and experiment would differ in magnitude, but are expected to be correlated. One can also note that the calculated permeabilities vary by orders of magnitude,

ranging from 10^{-5} - 10^{-14} cm s^{-1} , compared to a relatively narrow range obtained from experiments (10^{-4}-10^{-5} cm s^{-1}). In Fig. 2 we plotted the experimental (P_{exp}) and estimated permeabilities (P_{calc}) for the antibiotics on a logarithmic scale. While the predicted permeabilities for most of the antibiotics qualitatively follow the experimentally observed trend, a few exceptions with large deviations from the expected linear fit were noted. Out of the 4 antibiotics with the lowest P_{exp} ($\leq$ 1.0 x 10^{-5} cm s^{-1}), our approach predicted a relatively high P_{calc} for ampicillin (AMP), of the order of 10^{-7} cm s^{-1}, compared to benzylpenicillin (BPN), cephaloram (CFR) and cefamandole (CFM) with permeability values of the order of 10^{-12}-10^{-14} cm s^{-1} (Table 1). Similarly, among the faster permeating antibiotics in the set, a very low P_{calc} was obtained for cefazolin (CFZ) (of the order of 10^{-14} cm s^{-1}).

In the context of these observed outliers, it is interesting to compare CFZ with CFR, both mono-anionic antibiotics. While the molecular weight of CFZ of 453 is greater than that of CFR, i.e., 389, the permeability of CFZ is about 20-fold greater than that of CFR. Previously, Nikaido et al. (63) reported that this large difference in the permeation rates is due to the negative effect of hydrophobicity of the molecule on the permeation rate. CFZ is more hydrophilic (logP=-1.52) than CFR (logP=0.10) which would explain the greater permeability value for the former in experiments. Although, our method predicts a slightly larger permeability for CFZ than for CFR, the predicted value is low by a large margin. The reason for this deviation is not clear, but is likely due to the inability of the implicit scheme in adequately capturing the molecular behavior in this instance. Note that Ferriera and Kasson were able to predict the permeability of CFZ within the experimental range using all-atom classical MD simulations (22). In case of AMP, we find that the method predicts a permeation rate that is similar in the order of magnitude to other zwitterionic antibiotics in the set. In general, zwitterionic molecules have been reported to permeate much faster than anionic molecules belonging to a similar class of antibiotics (10). The low experimental permeability for AMP is therefore a bit surprising. For instance, comparing AMP, PIP and BPN, AMP (zwitterionic) is expected to permeate faster than PIP (anionic) and BPN (anionic). This trend is also predicted from the TABD calculations. However, different studies have provided contradicting estimates of relative permeabilities for AMP, PIP and BPN. While the experimental data used in this study indicates a larger permeability for PIP compared to AMP, another study has reported a larger permeability for AMP (10). Similarly, previous studies have reported a higher relative permeability for BPN compared to AMP (22, 67) that contradicts the findings of Kojima and Nikaido (66). These discrepancies suggest that the results are prone to experimental errors and are most likely influenced by the different assay conditions. We also note here that for the present analysis, the experimental data has been collected from independent studies as has been done earlier (22). It is expected that the experimental values are at least able to capture a general trend in the relative permeability values. Furthermore, it is important to note that owing to the approximate scheme used for obtaining the computed free energies and solute diffusion constants inside the channel in the present BD based scheme, our focus is to examine the performance of the scheme in reproducing the overall trend in the permeability rates. Under these conditions, the approach is able to capture fairly well the observed trend in the experimental

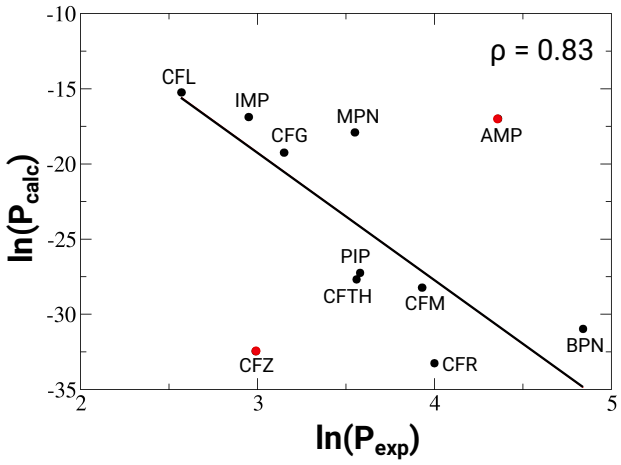

Figure 2: Validation of estimated against experimental drug permeabilities. The calculated drug permeabilities are depicted in a log-log plot against previously reported experimental data (see also Tab. 1) . The outlier cases are depicted in red. The line represents a linear fit of the data excluding the outlier points. The Pearson correlation coefficient ρ calculated for the black points is shown in the upper right corner of the graph.

permeabilities with a Pearson correlation coefficient of 0.83.

Molecule	Charge	Mol. wt.	Globularity	RBonds	Accumulation rate(nmol/10^{12}CFUs)	P_{calc} X 10^{-5}cm s^{-1}	R.E.
M1	+	145	0.24	0	0	6.59 x 10^{-2}	0.16
M2	+ +	144	0.17	0	20	9.96 x 10^{-8}	0.22
M3	+ - - -	415	0.19	7	52	3.51 x 10^{-8}	0.38
M4	-	284	0.18	1	56	3.85 x 10^{-7}	0.12
M5	-	512	0.19	5	56	N.A.	N.A.
M6	o	279	0.19	1	65	3.28 x 10^{-2}	0.16
M7	+ -	335	0.19	1	91	4.71 x 10^{-2}	0.17
M8	o	226	0.12	6	139	3.68 x 10^{-2}	0.14
M9	+	324	0.21	8	141	9.73 x 10^{-2}	0.16
M10	o	301	0.12	3	193	4.07 x 10^{-2}	0.12
M11	+ -	285	0.14	1	238	1.06 x 10^{-2}	0.23
M12	+	250	0.12	4	399	4.57 x 10^{-3}	0.35
M13	+	183	0.06	1	617	4.48 x 10^{-4}	0.12
M14	+	163	0.12	2	726	4.81 x 10^{-4}	0.16
M15	+	153	0.36	0	761	9.09 x 10^{-5}	0.39
M16	+	311	0.14	2	922	1.17 x 10^{-4}	0.43
M17	+ +	270	0.21	1	946	5.38 x 10^{-3}	0.24
M18	+	364	0.11	3	1647	1.67 x 10^{-1}	0.10
M19	+	444	0.20	2	1759	8.23 x 10^{-2}	0.19
M20	+	283	0.20	2	1887	1.13	0.12
M21	+	361	0.06	4	1965	1.66	0.11
M22	+ -	331	0.07	3	2263	5.11 x 10^{-2}	0.31

Table 2: Molecules selected for validation against whole cell accumulation rates in *E.coli* as reported previously (9). The estimates for permeability of each molecule obtained from TABD calculations is also provided. Note that in case of M5 the P_{calc} values could not be estimated due to incomplete sampling (see Figure S4). The charge column depicts the charged moieties present on the molecule with 'o' specifying the absence of charged moieties.

As additional validation, we also considered experimental data on accumulation rates in *E.coli*. Although, results of accumulation assays can be influenced by a number of factors such as antibiotic efflux rates, (non)specific binding and assay protocol, antibiotic accumulation rates are in general suggestive of the permeation efficiency. For the present analysis, we carefully selected 22 molecules out of the whole cell accumulation data reported in a previous study (9). Specifically, we included molecules that cover the full range of accumulation rates observed in that study (0 - 2263 nmol/10^{12} CFUs) and that includes zwitterionic, charged and uncharged molecules (Tab. 2 and Fig. S7). The set contains 13 anionic molecules that vary in terms of number of anionic moieties, molecular weight, globularity and rotatable bonds to ensure a large variability in physico-chemical parameters shown to influence accumulation rates. TABD simulations using a temperature of 1000 K were performed on this set to obtain 1D free energy plots as shown in Fig. S8. From these free energy profiles permeabilities were predicted. Plotting $ln(P_{calc})$ against the accumulation rate, we note that the predicted permeabilities for most of the molecules are fairly correlated with the accumulation rate as shown in Fig. 3. However, 6 out of the 22 tested molecules show large deviations (depicted in red in Fig. 3). All six molecules showed negligible to low accumulation rates in experiment but are predicted to be fast permeators from our calculations. Within these outliers, two molecules (M1 and M9) contain a primary amine, and one is zwitterionic (M7). Previously, fitting a large set of molecular descriptors to the accumulation data, Hergenrother and coworkers (9) had suggested that molecules with primary amines are more likely to permeate faster, but also noted that the presence of a primary amine is not sufficient and other factors such as globularity, hydrophobicity, and the number of rotatable bonds influence the accumulation. From the approximate one-dimensional free energy estimates based on the TABD runs, it appears that these molecules encounter a relatively shallow free energy landscape during permeation (see Fig. S7). This would suggest a possibility that the low accumulation rate noted in the assays is likely due to fast bidirectional translocation through the porins, that would lead to a net low accumulation within the cell. Similarly, the deviating molecules M6, M8 and M10 are uncharged neutral molecules with predicted high permeation rates compared to the very low accumulation observed in experiments. In these cases too, we note a shallow free energy landscape for permeation. These outliers highlight that an accumulation rate as calculated in experiments is not an indicator of the rate of influx within the cell, but that of the net effect of the influx and efflux processes. These results suggest that the present approach based on fast TABD simulations can provide semi-quantitative, preliminary data on the permeability of a molecule through porins, and can possibly uncover cases

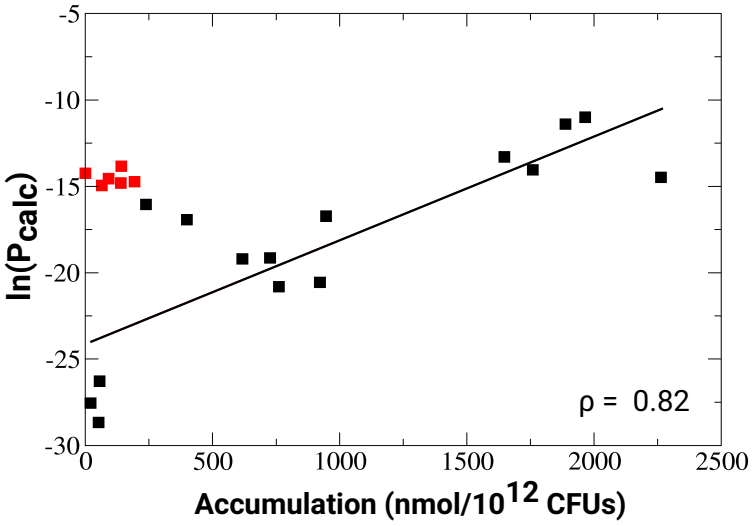

Figure 3: Correlation with experimental accumulation rates. Experimental intracellular accumulation rates are reported as concentration of the solute (in nanomoles) per 10^{12} colony forming units (CFUs). The calculated log of drug permeabilities are plotted against previously reported accumulation rates (9). The outliers points are depicted in red. The line depicts a linear fit to the data excluding the outlier points and ρ denotes the Pearson correlation coefficient for the set excluding the outlier points in red.

wherein accumulation rates may not correlate with the permeability rates.

One of the practical use cases for the present approach could be the screening of chemically modified variants of a parent molecule for those altered molecules with improved permeation properties. We therefore examined the potential of the present approach in predicting the effect of molecular transformations on the permeability of the resulting molecule. A recent study analyzed a carefully curated MIC dataset on experimentally investigated compounds obtained from the ChEMBL database and identified a number of chemical transformations that are associated with improved antibacterial activity against Gram-negative pathogens (19). At the outset, one must note that a demonstrated correlation between a given set of chemical transformations and improved antibacterial activity does not necessarily mean that the transformations are relevant to the permeability process. The changes in antibacterial activity may also be, for instance, a result of stronger affinity to an intracellular target. Notably among other transformations, the authors identified the addition of a primary amine group favoring the conversion of a Gram-negative inactive compound to Gram-negative active compound, which has been reported independently to favor the accumulation of compounds via accumulation assays (9, 11, 15). For the present analysis, we selected a set of 10 example transformation pairs (molecule A to molecule B) that involve the addition of a primary amine and are associated with an improved activity against Gram-negative bacteria (Tab. 3 and Fig. S9), with the assumption that these transformations lead to improvements in the antibacterial activity primarily as a result of higher permeability. In particular, we screened the chemical transformation dataset available from the previous study to obtain a subset associated with the introduction of a primary amine and a significant increase in the associated pMIC values, Δ pMIC$\geq$2.0 (see also Methods and Fig. S1). It is important to note that all transformation pairs are essentially chemical modifications around the fluoroquinolone bicyclic core and involve a chemical transformation more complex than a simple introduction of a primary amine moiety. As such these transformations represent realistic cases of molecular modifications that may be expected in a drug optimization effort. The permeability estimates for these transformation pairs show that the method predicts a greater permeation for molecule B compared to molecule A for all transformation pairs except for the pair T8. Note that for a number of pairs, no permeation was observed for molecule A (indicated by N.A. in Tab. 3). For each of these pairs, the method predicted significantly improved permeability for molecule B. For some pairs, the increase in predicted permeability was much lower, e.g. pairs T2 and T9. Overall, the predictions were found to largely agree with the expectations within the aforementioned assumptions.

Molecule A (ID)	pMIC	$P^{A}_{calc} \cdot 10^{-5}$ cm s^{-1}	R.E.	Molecule B (ID)	pMIC	$P^{B}_{calc} \cdot 10^{-5}$ cm s^{-1}	R.E.	Prediction
T1A (6191)	3.95	1.26 x 10^{-6}	0.87	T1B (1274)	7.81	1.79 x 10^{-5}	0.91	✓
T2A (6212)	3.53	1.01 x 10^{-5}	1.04	T2B (1183)	7.50	1.30 x 10^{-5}	0.87	✓
T3A (6804)	3.55	N.A.	N.A.	T3B (2259)	7.51	2.03 x 10^{-5}	0.91	✓
T4A (6162)	3.56	N.A.	N.A.	T4B (2259)	7.51	2.03 x 10^{-5}	0.91	✓
T5A (6746)	4.20	N.A.	N.A.	T5B (3392)	7.36	4.73 x 10^{-5}	0.76	✓
T6A (6745)	4.26	N.A.	N.A.	T6B (2500)	7.19	2.32 x 10^{-5}	1.11	✓
T7A (6745)	4.26	N.A.	N.A.	T7B (2479)	7.29	6.77 x 10^{-6}	0.94	✓
T8A (6933)	4.86	2.70 x 10^{-3}	0.75	T8B (4310)	7.70	1.06 x 10^{-6}	0.94	x
T9A (147)	5.08	2.24 x 10^{-5}	0.75	T9B (149)	7.10	1.44 x 10^{-4}	0.82	✓
T10A (466)	6.02	2.10 x 10^{-8}	0.16	T10B (4311)	7.98	4.49 x 10^{-5}	0.81	✓

Table 3: Permeability predictions corresponding to 10 molecular transformation pairs. For each pair of transformation we examined if the BD approach predicts an increase in permeation rate. The rightmost column specifies if the prediction agrees with the expectation that the introduction of a primary amine improved permeation, as is also predicted based on pMIC values. Here, the pMIC value is defined as pMIC= $-\log(\text{MIC } [\mu\ M] \text{ x } 10^{-6})$ with values obtained from the dataset in Ref. 19. R.E. denotes the relative error calculated as $\Delta\ P_{calc}/P_{calc}$.

CONCLUSION

The efforts towards the development of potent and broad spectrum antibiotic molecules focus on the identification of novel compounds against new targets and improvements in the efficacy of existing antibiotics. A significant bottleneck in translating potential inhibitors to potent antibiotics has been the low net accumulation of antibiotics either due to low rates of influx across Gram-negative bacterial membrane or high efflux rates mediated by bacterial efflux pumps. Improvements in influx rates is one possible approaches towards enhancing the net accumulation and the antibacterial activity. A fast computational prediction of molecular permeability through porin channels would aid significantly the efforts towards a high-throughput screening for potential drug candidates that can permeate efficiently. Here we present a Brownian dynamics based approach with explicit atoms (BRODEA) that significantly reduces the computational burden necessary for estimating permeabilities compared to previous approaches with an acceptable reproduction of observed trends in experimental permeabilities and accumulation rates. We note that for these simulations, an average performance of 155 μs/day was obtained on a single node with two Intel Xeon Platinum 9242 processors and each run required about 8-12 hrs of wall time. The setup procedure for each run, including, the generation of precomputed grids for the Poisson-Boltzmann electrostatics and the reaction-field required an additional 1 hr of wall time per run. This is significantly lower than previously reported wall time of a week per molecule. Concomitantly, the economic cost of predicting the permeability of a molecule is reduced to approximately $43 compared to $1318 in an earlier study that employed all-atom MD simulations (22). The estimate is based on the specified usage charges of $3.64 per node per hour within the applied compute project. The approach thus permits high-throughput calculations of permeabilities for a large molecule library through a straightforward parallelization. Another practical advantage is the minimal expert intervention needed in setting up the actual TABD simulations for individual molecules, the limiting step, is now reduced to the generation of appropriate force-field parameters for each molecule. The previously reported umbrella sampling-based approach, for instance, for each molecule requires a careful setup of the initial configurations for the simulation windows using steered MD and involves the optimization of the pulling rates introducing additional computational and human effort (22).

At the same time, the present approach makes some simplifying assumptions in its treatment of the problem of predicting antibiotic permeabilities. Foremost is the one-dimensional treatment of the solute diffusion problem through the application of the ISD model. As discussed, the permeability calculated is effectively pertains to the behaviour of a single channel, and not the permeability of a unit area of a bacterial membrane patch, as is reported in experimental studies. We use Eq. 6 to calculate the channel permeability for a given molecule. Here too, the BD simulations are used to calculate the $F(z)$ term limited to the region $z \in$ [-24Å , 20Å] within the channel. The term $D(z)$ is also estimated using the hydrodynamic model that relates the ratio $R_h/R_{pore}(z)$ to $D(z)$. Furthermore, the BD scheme has some technical limitations in terms of the treatment of protein dynamics that is also critical for antibiotic permeation through the channel (68, 69). The strategy employed herein utilizes rigid electrostatic potential maps for representing the channel. The MCRI scheme attempts to improve this by allowing multiple input configurations, but induced fluctuations of loops and side chains in presence of antibiotics are still not captured by the approach, which may present difficulties in obtaining sufficient sampling in the narrow constriction region as observed for some of the bulky antibiotics in our dataset. This limitation may be circumvented by increasing the temperature used for the TABD run, but in our view, is only a stopgap remedy to the issue. With the availability of increasingly powerful processors, future efforts could start by introducing additional protein atoms as explicit particles, especially the atoms of the constriction loop, which is possible within the BRODEA approach (32, 33) in combination with the use of multiple initial channel configurations obtained from a prior MD simulation.

An interesting finding has been the possibility of identifying cases wherein the experimental reports of accumulation rates

may not reflect the permeability of the molecule. The predictions could be useful in informing experimentalists about possible problematic cases that require careful consideration. At the same time, one can consider the results obtained from the recent analysis of MIC datasets regarding possible molecular transformations that lead to increase/decrease in MIC (19). Although, the study revealed a number of transformations that improve or reduce antibacterial efficacy against Gram-negative bacteria, it is not clear to what extent these transformations are relevant to the permeation process, i.e. influx vs efflux. It would be interesting to perform more detailed investigations on other predicted transformations to obtain statistically meaningful data on their influence on the influx rates. Overall, the BRODEA-based TABD approach enables the fast and approximate prediction of the permeability of a given molecule through a channel and could be used for preliminary screening of a large library of compounds and the effect of chemical modifications on the permeation rates. Incorporation of the approach at specific stages of the antibiotic development efforts could prove to be useful for optimizing the accumulation of the compounds of interest within the bacterial cell, in a similar manner as docking approaches in ligand design.

AUTHOR CONTRIBUTIONS

U.K. conceived the research together with A.A. The computational work was carried out by A.A. and K.J. with specific inputs from D.G and U.Z. on the work on molecular transformations. A.A. and U.K wrote the manuscript with input from K.J., D.G. and U.Z.; A.A. and K.J. contributed equally to the entire work.

DECLARATION OF INTERESTS

The authors declare no competing interests.

ACKNOWLEDGMENTS

A.A., K.J. and U.K. gratefully acknowledge financial support by the Deutsche Forschungsgemeinschaft (DFG) through project KL-1299/22-1. D.G. and U.Z. were supported by funding from the MRC (iCASE award MR/R015791/1 together with Helperby Ltd.). Computing time from the Norddeutscher Verbund für Hoch- und Höchstleistungsrechnen (HLRN) through project hbp00068 is gratefully acknowledged. A.A. and U.K. acknowledge Jigneshkumar Dahyabhai Prajapati for helpful discussions on the BRODEA scheme and software.

REFERENCES

1. Nikaido, H., 1994. Prevention of Drug Access to Bacterial Targets: Permeability Barriers and Active Efflux. *Science* 264:382–388.

2. Nikaido, H., 2003. Molecular Basis of Bacterial Outer Membrane Permeability Revisited. *Microbiol. Mol. Biol. Rev.* 67:593–656.

3. Tommasi, R., D. G. Brown, G. K. Walkup, J. I. Manchester, and A. A. Miller, 2015. ESKAPEing the Labyrinth of Antibacterial Discovery. *Nat. Rev. Drug Discov.* 14:529–542.

4. Ghai, I., M. Winterhalter, and R. Wagner, 2017. Probing Transport of Charged β-Lactamase Inhibitors through OmpC, a Membrane Channel from *E. coli*. *Biochem. Biophys. Res. Comm.* 484:51–55.

5. Bajaj, H., S. Acosta-Gutiérrez, I. Bodrenko, G. Malloci, M. A. Scorciapino, M. Winterhalter, and M. Ceccarelli, 2017. Bacterial Outer Membrane Porins As Electrostatic Nanosieves: Exploring Transport Rules of Small Polar Molecules. *ACS Nano* 11:5465–5473.

6. Samanta, S., I. Bodrenko, S. Acosta-Gutiérrez, T. D'Agostino, M. Pathania, I. Ghai, C. Schleberger, D. Bumann, R. Wagner, M. Winterhalter, B. van den Berg, and M. Ceccarelli, 2018. Getting Drugs through Small Pores: Exploiting the Porins Pathway in *Pseudomonas aeruginosa*. *ACS Infect. Dis.* 4:1519–1528.

7. Vergalli, J., I. V. Bodrenko, M. Masi, L. Moynié, S. Acosta-Gutiérrez, J. H. Naismith, A. Davin-Regli, M. Ceccarelli, B. Van Den Berg, M. Winterhalter, and J.-M. Pagès, 2020. Porins and Small-Molecule Translocation across the Outer Membrane of Gram-Negative Bacteria. *Nat. Rev. Microbiol.* 18:164–176.

8. Prajapati, J. D., U. Kleinekathöfer, and M. Winterhalter, 2021. How to Enter a Bacterium: Bacterial Porins and the Permeation of Antibiotics. *Chem. Rev.* 121:5158–5192.

9. Richter, M. F., B. S. Drown, A. P. Riley, A. Garcia, T. Shirai, R. L. Svec, and P. J. Hergenrother, 2017. Predictive Compound Accumulation Rules Yield a Broad-Spectrum Antibiotic. *Nature* 545:299–304.

10. Acosta-Gutiérrez, S., L. Ferrara, M. Pathania, M. Masi, J. Wang, I. Bodrenko, M. Zahn, M. Winterhalter, R. A. Stavenger, J.-M. Pagès, J. H. Naismith, B. van den Berg, M. G. P. Page, and M. Ceccarelli, 2018. Getting Drugs into Gram-Negative Bacteria: Rational Rules for Permeation through General Porins. *ACS Infect. Dis.* 4:1487–1498.

11. Richter, M. F., and P. J. Hergenrother, 2019. The Challenge of Converting Gram-Positive-Only Compounds into Broad-Spectrum Antibiotics. *Ann. N. Y. Acad. Sci.* 1435:18–38.

12. Parker, E. N., B. S. Drown, E. J. Geddes, H. Y. Lee, N. Ismail, G. W. Lau, and P. J. Hergenrother, 2020. Implementation of Permeation Rules Leads to a FabI Inhibitor with Activity against Gram-Negative Pathogens. *Nat. Microbiol.* 5:67–75.

13. Motika, S. E., R. J. Ulrich, E. J. Geddes, H. Y. Lee, G. W. Lau, and P. J. Hergenrother, 2020. Gram-Negative Antibiotic Active Through Inhibition of an Essential Riboswitch. *J. Am. Chem. Soc.* 142:10856–10862.

14. Perlmutter, S. J., E. J. Geddes, B. S. Drown, S. E. Motika, M. R. Lee, and P. J. Hergenrother, 2021. Compound Uptake into *E. coli* Can Be Facilitated by N-Alkyl Guanidiniums and Pyridiniums. *ACS Infect. Dis.* 7:162–173.

15. Parker, E. N., B. N. Cain, B. Hajian, R. J. Ulrich, E. J. Geddes, S. Barkho, H. Y. Lee, J. D. Williams, M. Raynor, D. Caridha, A. Zaino, M. Shekhar, K. A. Muñoz, K. M. Rzasa, E. R. Temple, D. Hunt, X. Jin, C. Vuong, K. Pannone, A. M. Kelly, M. P. Mulligan, K. K. Lee, G. W. Lau, D. T. Hung, and P. J. Hergenrother, 2022. An Iterative Approach Guides Discovery of the FabI Inhibitor Fabimycin, a Late-Stage Antibiotic Candidate with *In Vivo* Efficacy against Drug-Resistant Gram-Negative Infections. *ACS Central Science* 8:1145–1158.

16. Yang, Y. I., Q. Shao, J. Zhang, L. Yang, and Y. Q. Gao, 2019. Enhanced Sampling in Molecular Dynamics. *J. Chem. Phys.* 151:070902.

17. Stokes, J. M., K. Yang, K. Swanson, W. Jin, A. Cubillos-Ruiz, N. M. Donghia, C. R. Macnair, S. French, L. A. Carfrae, Z. Bloom-Ackerman, V. M. Tran, A. Chiappino-Pepe, A. H. Badran, I. W. Andrews, E. J. Chory, G. M. Church, E. D. Brown, T. S. Jaakkola, R. Barzilay, and J. J. Collins, 2020. A Deep Learning Approach to Antibiotic Discovery. *Cell* 180:688–702.e13.

18. Dossetter, A. G., E. J. Griffen, and A. G. Leach, 2013. Matched Molecular Pair Analysis in Drug Discovery. *Drug Discov. Today* 18:724–731.

19. Gurvic, D., A. G. Leach, and U. Zachariae, 2022. Data-Driven Derivation of Molecular Substructures That Enhance Drug Activity in Gram-Negative Bacteria. *J. Med. Chem.* 65:6088–6099.

20. Acharya, A., J. D. Prajapati, and U. Kleinekathöfer, 2022. Atomistic Simulation of Molecules Interacting with Biological Nanopores: From Current Understanding to Future Directions. *J. Phys. Chem. B* 126:3995–4008.

21. Marrink, S.-J., and H. J. C. Berendsen, 1994. Simulation of Water Transport through a Lipid Membrane. *J. Phy. Chem.* 98:4155–4168.

22. Ferreira, R. J., and P. M. Kasson, 2019. Antibiotic Uptake Across Gram-Negative Outer Membranes: Better Predictions Towards Better Antibiotics. *ACS Infect. Dis.* 5:2096–2104.

23. Im, W., S. Seefeld, and B. Roux, 2000. A Grand Canonical Monte Carlo-Brownian Dynamics Algorithm for Simulating Ion Channels. *Biophys. J.* 79:788–801.

24. Im, W., and B. Roux, 2001. Brownian Dynamics Solutions of Ions Channels: A General Treatment of Electrostatic Reaction Fields for Molecular Pores of Arbitrary Geometry. *J. Chem. Phys.* 115:4850.

25. Im, W., and B. Roux, 2002. Ion Permeation and Selectivity of OmpF Porin: A Theoretical Study Based on Molecular Dynamics, Brownian Dynamics, and Continuum Electrodiffusion Theory. *J. Mol. Biol.* 322:851–869.

26. Noskov, S., W. Im, and B. Roux, 2004. Ion Permeation through the α-Hemolysin Channel: Theoretical Studies Based on Brownian Dynamics and Poisson-Nernst-Plank Electrodiffusion Theory. *Biophys. J.* 87:2299–2309.

27. Gillespie, D., 2008. Energetics of Divalent Selectivity in a Calcium Channel: The Ryanodine Receptor Case Study. *Biophys. J.* 94:1169–1184.

28. Boda, D., D. Henderson, and D. Gillespie, 2013. The Role of Solvation in the Binding Selectivity of the L-Type Calcium Channel. *J. Chem. Phys.* 139:055103.

29. Choudhary, A., H. Joshi, H.-Y. Chou, K. Sarthak, J. Wilson, C. Maffeo, and A. Aksimentiev, 2020. High-Fidelity Capture, Threading, and Infinite-Depth Sequencing of Single DNA Molecules with a Double-Nanopore System. *ACS Nano* 14:15566–15576.

30. Choudhary, A., C. Maffeo, and A. Aksimentiev, 2022. Multi-Resolution Simulation of DNA Transport through Large Synthetic Nanostructures. *Phys. Chem. Chem. Phys.* 24:2706–2716.

31. Lee, K. I., H. Rui, R. W. Pastor, and W. Im, 2011. Brownian Dynamics Simulations of Ion Transport through the VDAC. *Biophys. J.* 100:611–619.

32. Solano, C. J. F., K. R. Pothula, J. D. Prajapati, P. M. De Biase, S. Y. Noskov, and U. Kleinekathöfer, 2016. BROMOCEA Code: An Improved Grand Canonical Monte Carlo/Brownian Dynamics Algorithm Including Explicit Atoms. *J. Chem. Theory Comput.* 12:2401–2417.

33. Solano, C. J. F., J. D. Prajapati, K. R. Pothula, and U. Kleinekathöfer, 2018. Brownian Dynamics Approach Including Explicit Atoms for Studying Ion Permeation and Substrate Translocation across Nanopores. *J. Chem. Theory Comput.* 14:6701–6713.

34. Golla, V. K., J. D. Prajapati, and U. Kleinekathöfer, 2021. Millisecond-Long Simulations of Antibiotics Transport through Outer Membrane Channels. *J. Chem. Theory Comput.* 17:549–559.

35. Wang, J., J. D. Prajapati, U. Kleinekathöfer, and M. Winterhalter, 2020. Dynamic Interaction of Fluoroquinolone with Magnesium Ions Monitored by Bacterial Outer Membrane Nanopores. *Chem. Sci.* 11:10344–10353.

36. Brooks, B. R., C. L. Brooks, A. D. Mackerell, L. Nilsson, R. J. Petrella, B. Roux, Y. Won, G. Archontis, C. Bartels, S. Boresch, A. Caflisch, L. Caves, Q. Cui, A. R. Dinner, M. Feig, S. Fischer, J. Gao, M. Hodoscek, W. Im, K. Kuczera, T. Lazaridis, J. Ma, V. Ovchinnikov, E. Paci, R. W. Pastor, C. B. Post, J. Z. Pu, M. Schaefer, B. Tidor, R. M. Venable, H. L. Woodcock, X. Wu, W. Yang, D. M. York, and M. Karplus, 2009. CHARMM: The Biomolecular Simulation Program. *J. Comp. Chem.* 30:1545–1614.

37. Maragliano, L., and E. Vanden-Eijnden, 2006. A Temperature Accelerated Method for Sampling Free Energy and Determining Reaction Pathways in Rare Events Simulations. *Chem. Phys. Lett.* 426:168–175.

38. Vithani, N., P. K. Ankush Jagtap, S. K. Verma, R. Tripathi, S. Awasthi, N. N. Nair, and B. Prakash, 2018. Mechanism of Mg^{2+}-accompanied Product Release in Sugar Nucleotidyltransferases. *Structure* 26:459–466.e3.

39. Awasthi, S., S. Gupta, R. Tripathi, and N. N. Nair, 2018. Mechanism and Kinetics of Aztreonam Hydrolysis Catalyzed by Class-C β-Lactamase: A Temperature-Accelerated Sliced Sampling Study. *J Phys. Chem. B* 122:4299–4308.

40. Soniya, K., S. Awasthi, N. N. Nair, and A. Chandra, 2019. Transimination Reaction at the Active Site of Aspartate Aminotransferase: A Proton Hopping Mechanism through Pyridoxal 5'-Phosphate. *ACS Catal.* 9:6276–6283.

41. Acharya, A., J. D. Prajapati, and U. Kleinekathöfer, 2021. Improved Sampling and Free Energy Estimates for Antibiotic Permeation through Bacterial Porins. *J. Chem. Theory Comput.* 17:4564–4577.

42. Im, W., and B. Roux, 2002. Ions and Counterions in a Biological Channel: A Molecular Dynamics Simulation of OmpF Porin from *E*scherichia coli in an Explicit Membrane with 1 M KCl Aqueous Salt Solution. *J. Mol. Biol.* 319:1177–1197.

43. Zhu, F., and G. Hummer, 2012. Theory and Simulation of Ion Conduction in the Pentameric GLIC Channel. *J. Chem. Theory Comput.* 8:3759–3768.

44. Smith, G., and M. Sansom, 1999. Effective Diffusion Coefficients of K^+ and Cl^- Ions in Ion Channel Models. *Biophysical Chemistry* 79:129–151.

45. Smart, O. S., J. G. Neduvelil, X. Wang, B. A. Wallace, and M. S. P. Sansom, 1996. HOLE: A Program for the Analysis of the Pore Dimensions of Ion Channel Structural Models. *J. Mol. Graph.* 14:354–360.

46. Ortega, A., D. AmorÃ³s, and J. GarcÃaÂ deÂ laÂ Torre, 2011. Prediction of Hydrodynamic and Other Solution Properties of Rigid Proteins from Atomic- and Residue-Level Models. *Biophys. J.* 101:892–898.

47. Feenstra, K. A., B. Hess, and J. C. Berendsen, 1999. Improving Efficiency of Large Time-scale Molecular Dynamics Simulations of Hydrogen-rich Systems. *J. Comp. Chem.* 20:786–798.

48. Zhao, Y., and D. G. Truhlar, 2008. The M06 Suite of Density Functionals for Main Group Thermochemistry, Thermochemical Kinetics, Noncovalent Interactions, Excited States, and Transition Elements: Two New Functionals and Systematic Testing of Four M06-Class Functionals and 12 Other Functionals. *Theor. Chem. Acc.* 120:525–525.

49. Hariharan, P. C., and J. A. Pople, 1973. The Influence of Polarization Functions on Molecular Orbital Hydrogenation Energies. *Theor. Chim. Acta.* 28:213–222.

50. Pople, J., R. Ditchfield, and W. Hehre, 1971. Self-consistent Molecular-orbital Methods. IX. An Extended Gaussian-Type Basis for Molecular-orbital Studies of Organic Molecules. *J. Chem. Phys* 54:724–728.

51. Herbert, J. M., 2021. Dielectric Continuum Methods for Quantum Chemistry. *WIREs Comput. Mol. Sci.* 11:e1519.

52. Frisch, M. J., G. W. Trucks, H. B. Schlegel, G. E. Scuseria, M. A. Robb, J. R. Cheeseman, G. Scalmani, V. Barone, G. A. Petersson, H. Nakatsuji, X. Li, M. Caricato, A. V. Marenich, J. Bloino, B. G. Janesko, R. Gomperts, B. Mennucci, H. P. Hratchian, J. V. Ortiz, A. F. Izmaylov, J. L. Sonnenberg, D. Williams-Young, F. Ding, F. Lipparini, F. Egidi, J. Goings, B. Peng, A. Petrone, T. Henderson, D. Ranasinghe, V. G. Zakrzewski, J. Gao, N. Rega, G. Zheng, W. Liang, M. Hada, M. Ehara, K. Toyota, R. Fukuda, J. Hasegawa, M. Ishida, T. Nakajima, Y. Honda, O. Kitao, H. Nakai, T. Vreven, K. Throssell, J. A. Montgomery, Jr., J. E. Peralta, F. Ogliaro, M. J. Bearpark, J. J. Heyd, E. N. Brothers, K. N. Kudin, V. N. Staroverov, T. A. Keith, R. Kobayashi, J. Normand, K. Raghavachari, A. P. Rendell, J. C. Burant, S. S. Iyengar, J. Tomasi, M. Cossi, J. M. Millam, M. Klene, C. Adamo, R. Cammi, J. W. Ochterski, R. L. Martin, K. Morokuma, O. Farkas, J. B. Foresman, and D. J. Fox, 2016. Gaussian 16 Revision C.01. Gaussian Inc. Wallingford CT.

53. Vanommeslaeghe, K., E. Hatcher, C. Acharya, S. Kundu, S. Zhong, J. Shim, E. Darian, O. Guvench, P. Lopes, I. Vorobyov, and A. D. Mackerell, 2010. CHARMM General Force Field: A Force Field for Drug-like Molecules Compatible with the CHARMM All-Atom Additive Biological Force Fields. *J. Comput. Chem.* 31:671–690.

54. Yu, W., X. He, K. Vanommeslaeghe, and A. D. MacKerell, 2012. Extension of the CHARMM General Force Field to Sulfonyl-Containing Compounds and Its Utility in Biomolecular Simulations. *J. Comput. Chem.* 33:2451–2468.

55. CHARMM to Gromacs Topology Convert. http://mackerell.umaryland.edu/charmm_ff.shtml. Accessed 10-02-2022.

56. Becke, A. D., 1993. Density-functional Thermochemistry. III. The Role of Exact Exchange. *J. Chem. Phys.* 98:5648–5652.

57. Hummer, G., L. Pratt, and A. García, 1996. Free Energy of Ionic Hydration. *J. Phys. Chem.* 100:1206–1215.

58. Woolf, T. B., and B. Roux, 1994. Molecular Dynamics Simulation of the Gramicidin Channel in a Phospholipid Bilayer. *Proc. Natl. Acad. Sci. USA* 91:11631–11635.

59. Comer, J., C. Chipot, and F. D. González-Nilo, 2013. Calculating Position-Dependent Diffusivity in Biased Molecular Dynamics Simulations. *J. Chem. Theory Comput.* 9:876–882.

60. Lee, C. T., J. Comer, C. Herndon, N. Leung, A. Pavlova, R. V. Swift, C. Tung, C. N. Rowley, R. E. Amaro, C. Chipot, Y. Wang, and J. C. Gumbart, 2016. Simulation-Based Approaches for Determining Membrane Permeability of Small Compounds. *J. Chem. Inf. Model.* 56:721–733.

61. Mendez, D., A. Gaulton, A. P. Bento, J. Chambers, M. De Veij, E. Félix, M. Magariños, J. Mosquera, P. Mutowo, M. Nowotka, M. Gordillo-Marañón, F. Hunter, L. Junco, G. Mugumbate, M. Rodriguez-Lopez, F. Atkinson, N. Bosc, C. Radoux, A. Segura-Cabrera, A. Hersey, and A. Leach, 2018. ChEMBL: Towards Direct Deposition of Bioassay Data. *Nucleic Acids Res.* 47:D930–D940.

62. Dalke, A., J. Hert, and C. Kramer, 2018. mmpdb: An Open-Source Matched Molecular Pair Platform for Large Multiproperty Data Sets. *J. Chem. Inf. Model.* 58:902–910.

63. Nikaido, H., E. Y. Rosenberg, and J. Foulds, 1983. Porin Channels in Escherichia Coli: Studies with Beta-Lactams in Intact Cells. *J. Bacteriol.* 153:232–240.

64. Matsumura, N., S. Minami, Y. Watanabe, S. Iyobe, and S. Mitsuhashi, 1999. Role of Permeability in the Activities of β-Lactams against Gram-Negative Bacteria Which Produce a Group 3 β-Lactamase. *Antimicrob. Agents Chemother.* 43:2084–2086.

65. Liu, W., and H. Nikaido, 1991. Contribution of the Cell-Surface-Associated Enzyme in the Zimmermann-Rosselet Assay of Outer Membrane Permeability of Beta-Lactam Antibiotics. *Antimicrob. Agents Chemother.* 35:177–179.

66. Kojima, S., and H. Nikaido, 2013. Permeation Rates of Penicillins Indicate That Escherichia Coli Porins Function Principally As Nonspecific Channels. *Proc. Nat. Acad. Sci.* 110:E2629–E2634.

67. Hajjar, E., A. Bessonov, A. Molitor, A. Kumar, K. R. Mahendran, M. Winterhalter, J.-M. Pages, P. Ruggerone, and M. Ceccarelli, 2010. Toward Screening for Antibiotics with Enhanced Permeation Properties through Bacterial Porins. *Biochemistry* 49:6928–6935.

68. Vasan, A. K., N. Haloi, R. J. Ulrich, M. E. Metcalf, P.-C. Wen, W. W. Metcalf, P. J. Hergenrother, D. Shukla, and E. Tajkhorshid, 2022. Role of Internal Loop Dynamics in Antibiotic Permeability of Outer Membrane Porins. *Proc. Natl. Acad. Sci.* 119:e2117009119.

69. Acharya, A., I. Ghai, C. Piselli, J. D. Prajapati, R. Benz, M. Winterhalter, and U. Kleinekathöfer, 2023. Conformational Dynamics of Loop L3 in OmpF: Implications toward Antibiotic Translocation and Voltage Gating. *J. Chem. Inf. Model.* 63:910–927.

SUPPLEMENTARY MATERIAL

An online supplement to this article can be found by visiting BJ Online at http://www.biophysj.org.